STAR FORMATION IN THE NEARBY UNIVERSE: THE ULTRAVIOLET AND INFRARED POINTS OF VIEW

J. Iglesias-Páramo,[1,2] V. Buat,[1] T. T. Takeuchi,[1] K. Xu,[3] S. Boissier,[4] A. Boselli,[1] D. Burgarella,[1]
B. F. Madore,[4] A. Gil de Paz,[4] L. Bianchi,[5] T. A. Barlow,[3] Y.-I. Byun,[6] J. Donas,[1] K. Forster,[3]
P. G. Friedman,[3] T. M. Heckman,[7] P. N. Jelinski,[8] Y.-W. Lee,[6] R. F. Malina,[1] D. C. Martin,[3]
B. Milliard,[1] P. F. Morrissey,[3] S. G. Neff,[9] R. M. Rich,[10] D. Schiminovich,[3] M. Seibert,[3]
O. H. W. Siegmund,[8] T. Small,[3] A. S. Szalay,[7] B. Y. Welsh,[8] AND T. K. Wyder[3]
Received 2005 April 15; accepted 2006 January 10

ABSTRACT

This work presents the main ultraviolet (UV) and far-infrared (FIR) properties of two samples of nearby galaxies selected from the *GALEX* ($\lambda = 2315$ Å, hereafter NUV) and *IRAS* ($\lambda = 60$ μm) surveys, respectively. They are built in order to obtain detection at both wavelengths for most of the galaxies. Star formation rate (SFR) estimators based on the UV and FIR emissions are compared. Systematic differences are found between the SFR estimators for individual galaxies based on the NUV fluxes corrected for dust attenuation and on the total IR luminosity. A combined estimator based on NUV and IR luminosities seems to be the best proxy over the whole range of values of SFR. Although both samples present similar average values of the birthrate parameter b, their star-formation-related properties are substantially different: NUV-selected galaxies tend to show larger values of b for lower masses, SFRs, and dust attenuation, supporting previous scenarios of star formation history (SFH). Conversely, about 20% of the FIR-selected galaxies show high values of b, SFR, and NUV attenuation. These galaxies, most of them being LIRGs and ULIRGs, break down the downsizing picture of SFH; however, their relative contribution per unit volume is small in the local universe. Finally, the cosmic SFR density of the local universe is estimated in a consistent way from the NUV and IR luminosities.

Subject headings: infrared: galaxies — surveys — ultraviolet: galaxies

Online material: color figures, machine-readable tables

1. INTRODUCTION

What is the best way to measure the SFR of galaxies on large scales and at different redshifts? The ability to estimate the SFR of a galaxy directly from the luminosity at a single wavelength would be a major advantage for anyone wanting to compute the SFR per unit volume at a given redshift. This quantity could be derived directly from the luminosity function (LF) at this wavelength and redshift. Under these conditions, large-area surveys at single wavelengths might suffice.

The recent SFR of a galaxy is often measured from the light emitted by young stars: given their short lifetimes, their luminosity is directly proportional to the rate at which they are currently forming. The UV and FIR luminosities of star-forming galaxies are both closely related to recent star formation: most of the UV photons are originally emitted by stars younger than $\sim 10^8$ yr, but many of these photons are reprocessed by the dust present in galaxies and re-emitted at FIR wavelengths. Strictly

speaking, neither of these fluxes can be used alone to estimate the SFR independently of the other one (e.g., Buat & Xu 1996; Hirashita et al. 2003; Iglesias-Páramo et al. 2004). Because of the previous lack of data at both wavelengths, attempts have been made using only the rest-frame UV (Lilly et al. 1996; Madau et al. 1996; Steidel et al. 1999; and more recently Schiminovich et al. 2005 with *GALEX* data) or just FIR data (Rowan-Robinson et al. 1997; Chary & Elbaz 2001), but only a few authors have compared both (Flores et al. 1999; Cardiel et al. 2003). The SFR estimator based on the UV luminosity suffers from attenuation by dust, and it has to be corrected in order to properly trace the SFR: for UV-selected samples of galaxies, the attenuation can reach more than 1 mag (e.g., Iglesias-Páramo et al. 2004; Buat et al. 2005). On the other hand the FIR emission is not free of problems because the dust can also be heated by old stars and can be a nonnegligible correction for many star-forming galaxies (Lonsdale & Helou 1987; Sauvage & Thuan 1992). Neither of these two indicators taken alone is an accurate estimator of the SFR except perhaps for starburst galaxies, in which (1) the dust attenuation was found to follow a tight relation with the slope of the spectrum at UV wavelengths (Meurer et al. 1999), thus allowing one to estimate the dust attenuation with only information on UV fluxes, and (2) the contribution to the dust emission coming from old stars can be neglected (Sauvage & Thuan 1992). In the most general case, the best estimator of the SFR should contain combined information of the luminosities at both wavelength ranges (Hirashita et al. 2003). The UV and FIR fluxes are thus complementary for tracing star formation, and it is well known that the FIR/UV ratio is a proper indicator of the dust attenuation (Buat et al. 1999; Witt & Gordon 2000; Panuzzo et al. 2003). Although other indicators of the recent SFRs of galaxies have been extensively used in the literature, a detailed discussion of their quality as SFR tracers is not discussed in this paper.

[1] Laboratoire d'Astrophysique de Marseille, 13376 Marseille, France.

[2] Instituto de Astrofísica de Andalucía, Camino Bajo de Huetor 24, 18008 Granada, Spain.

[3] Space Astrophysics Laboratory, Mail Stop 405-47, California Institute of Technology, 1200 East California Boulevard, Pasadena, CA 91125.

[4] Observatories of the Carnegie Institution of Washington, 813 Santa Barbara Street, Pasadena, CA 91101.

[5] Center for Astrophysical Sciences, Johns Hopkins University, 3400 North Charles Street, Baltimore, MD 21218.

[6] Center for Space Astrophysics, Yonsei University, Seoul 120-749, South Korea.

[7] Department of Physics and Astronomy, Johns Hopkins University, Homewood Campus, Baltimore, MD 21218.

[8] Space Sciences Laboratory, University of California, 601 Campbell Hall, Berkeley, CA 94720.

[9] Laboratory for Astronomy and Solar Physics, NASA Goddard Space Flight Center, Greenbelt, MD 20771.

[10] Department of Physics and Astronomy, University of California, Los Angeles, CA 90095.

The *GALEX* (*Galaxy Evolution Explorer*) mission (Martin et al. 2005a) is imaging the high-Galactic-latitude sky at two UV wavelengths ($\lambda = 1530$ Å, *FUV*; $\lambda = 2315$ Å, *NUV*) and is providing the astronomical community with unprecedented data (both in quantity and quality). The UV data combined with existing FIR data sets (from the *IRAS* [*Infrared Astronomical Satellite*], *Infrared Space Observatory*, or *Spitzer* missions) now allow us to carry out detailed studies of the UV and FIR properties of galaxies, with special emphasis on the derivation of the dust attenuation and star formation activity in star-forming galaxies.

With this purpose in mind we have selected two samples of galaxies: one from the *GALEX* All-Sky Imaging Survey (AIS) and the other from the *IRAS* Point Source Catalog Redshift Survey (PSCz; redshifts, infrared and optical photometry, and additional information for 18,351 *IRAS* sources, mostly selected from the Point Source Catalog) and the Faint Source Catalog (FSC), for which UV and FIR fluxes are available. With these data sets in hand we have undertaken a study of the properties related to their emissions at these wavelengths. Both samples were extracted from the same region of the sky ($\sim$600 degrees^2, constrained by the status of the *GALEX* survey when this work was initiated). From the *GALEX* catalog we built a complete sample of galaxies down to $AB_{NUV} = 16$ mag[11] and cross-correlated it with the *IRAS* database (FSC), allowing nondetections at 60 μm (fluxes lower than 0.2 Jy). The FIR-selected sample was built from the *IRAS* catalog (PSCz) with a limiting flux at 60 μm of 0.6 Jy as the only constraint. The resulting list of PSCz sources was cross-correlated with the *GALEX* database, allowing again nondetections in the NUV. Both the NUV and the 60 μm limits used to build the samples were chosen to allow for a very small number of nondetections and to sample the galaxy population over a large range of values of the dust attenuation. Besides being useful for an analysis of the SFR, these NUV- and FIR-selected samples of galaxies (chosen with well-defined selection criteria) can also be used to place important constraints on models designed to predict the statistical properties of galaxy populations. The attenuation of star light by interstellar dust and its emission in the FIR are usually computed very crudely in models of galactic evolution. Dust attenuation is usually deduced in such approaches from other quantities such as the gas mass and the metallicity (e.g., Guiderdonni & Rocca-Volmerange 1987; Devriendt & Guiderdoni 2000; Balland et al. 2003). The properties of large samples of galaxies observed both in the UV and FIR with clear selection criteria, such as the ones presented in this paper, provide an important statistical constraint for the calibration of the treatment of dust in such models.

The first paper in the series (Buat et al. 2005) based on these samples was mainly devoted to dust attenuation properties. In the present work we discuss various aspects relating to the NUV and 60 μm emission of our sample galaxies, including systematic differences in the 60 μm and NUV luminosities, and we focus on their star-formation-related properties. This paper is organized as follows. The samples are presented in § 2, the relation between the NUV and 60 μm luminosities is discussed in § 3, and § 4 is devoted to the derivation of the SFR and to a comparison of various estimators, as well as to a discussion of the star formation activity related properties of the samples. The derivation of the local cosmic SFR density by different methods is discussed in § 5. The main conclusions are presented in § 6. Throughout this paper we adopt the following cosmological parameter set: (h, Ω_0, λ_0) = (0.7, 0.3, 0.7), where $h \equiv H_0/100$ km s^{-1}Mpc^{-1}.

2. OBSERVATIONAL DATA SET

2.1. *NUV-selected Sample*

In order to build the NUV-selected sample, we used 833 fields of the *GALEX* AIS, each having an exposure time equal to or larger than 50 s. We used only the central $0.^\circ5$ radius circles in each field to ensure a uniform image quality: the resulting sky coverage is 615 deg^2. Within this area we selected all the galaxies of the *GALEX* AIS survey with $AB_{NUV} \leq 16$ mag. This bright limit was chosen in order to ensure *IRAS* detections of all the galaxies with attenuation larger than $\sim$0.3 mag (for a limit of 0.2 Jy at 60 μm from the *IRAS* FSC using the calibration of Buat et al. 2005), and highly significant upper limits for the less attenuated galaxies.

On one hand, the moderate angular resolution of *GALEX* (FWHM $\sim 6''$) does not allow for a secure discrimination of stars from small galaxies. On the other hand, the *GALEX* pipeline can induce some shredding of larger galaxies. This results in multiple detections that (cumulatively) correspond to a single galaxy because of the misidentification of star-forming regions as individual galaxies. The main consequence of this is the underestimation of the fluxes of large galaxies. Corollary catalogs were thus required in order to perform a reliable selection of galaxies. Our starting point was the catalog of NUV detections produced by the *GALEX* pipeline,[12] which made use of the SExtractor code (Bertin & Arnouts 1996). We made the assumption that all the galaxies brighter than $AB_{NUV} = 16$ mag, even if they were shredded, should contain at least one SExtractor detection brighter than $AB_{NUV} = 18$ mag. Then we associated an object from databases of well-known stars and galaxies (SIMBAD, 2MASS [the Two Micron All Sky Survey], LEDA [the Lyon Extragalactic Database]) with each of the SExtractor detections brighter than $AB_{NUV} = 18$ mag. The problem of shredding was mostly resolved by using LEDA. As this database contains the optical diameters of the galaxies, NUV detections corresponding to shredded galaxies can be associated with their parent galaxies, provided they are located within the aperture defined by the optical diameters and the position angle listed in LEDA. For the detections of galaxies not shredded, we used SIMBAD and 2MASS in order to classify them as stars or galaxies. Finally, objects not associated with any known source were classified as "dubious." In order to test the quality of our selection method, we cross-correlated our final catalog with the SDSS Data Release 1, which spatially overlaps one-fifth of our sample. The spectral and photometric information of the SDSS, together with its higher angular resolution, made possible an optimal classification of all the objects detected in the field: all the objects present in both *GALEX* and SDSS catalogs were found to be properly classified. Dubious objects were found to be noise detections or ghosts generated mainly near the edges of the *GALEX* frames. Thus we ended up with a catalog of bona fide galaxies or fragments of galaxies (i.e., belonging to the large galaxies shredded by SExtractor) brighter than $AB_{NUV} = 18$ mag. The next step was to obtain aperture photometry of these objects in order to select out only the galaxies brighter than $AB_{NUV} = 16$ mag.

Photometry of our sample galaxies was performed in the *GALEX* NUV and FUV bands. Since the selection criterion for our sample galaxies was imposed in the NUV band, we also took the NUV images as our reference for the total photometry. We performed aperture photometry using a set of elliptical apertures, the total photometry corresponding to the aperture where

---

[11] AB magnitudes are defined as $AB_\nu = -2.5 \log f_\nu - 48.6$, where f_ν is the monochromatic flux density expressed in ergs s^{-1} cm^{-2} Hz^{-1}.

[12] Version 0.2.0, 2003 September, with the correction to NUV and FUV magnitudes reported in Buat et al. (2005).

AB Magnitude Interval	$\sigma(\mathrm{NUV})$ (mag)	$\sigma(\mathrm{FUV})$ (mag)
≤ 16	0.01	0.02
16–18	0.03	0.05
18–20	0.09	0.15
20–22	0.26	0.40

convergence of the growth curve is achieved. Once we determined the total NUV flux, the photometry in the FUV band was obtained by performing background-subtracted aperture photometry within the same elliptical aperture where convergence of the NUV growth curve was achieved. This way, the NUV − FUV colors are consistent. Some galaxies were contaminated by the flux of nearby bright stars or galaxies. The contaminating sources were then masked in the NUV and FUV frames in order to obtain proper NUV and FUV fluxes for our galaxies. Table 1 shows the typical uncertainties of the NUV and FUV magnitudes. NUV and FUV magnitudes were corrected for Galactic extinction using the Schlegel et al. (1998) dust map and the Cardelli et al. (1989) extinction curve. In the end, a total of 95 nonstellar objects brighter than $\mathrm{AB_{NUV}} = 16$ mag were found. One of them, classified as a QSO, was excluded from the sample.

FIR fluxes at 60 μm were obtained from the *IRAS* FSC (Moshir et al. 1990) for 68 of our 95 galaxies. We discarded all those sources for which the cirrus parameter (as listed by the FSC) is larger than 2 because it can result in uncertain fluxes. The Scan Processing and Integration Facility (SCANPI) was used to obtain the FIR fluxes for the remaining 27 objects. Three of these galaxies (UGC 11866, UGCA 438, and UGC 12613) were not detected at 60 μm. We adopted a conservative upper limit of 0.2 Jy at 60 μm (as given in the FSC) for these galaxies. Four galaxies of the sample were not covered by the *IRAS* survey.

2.2. FIR-selected Sample

The FIR-selected sample was extracted from the *IRAS* PSCz (Saunders et al. 2000) over the 509 deg^2 in common with the *GALEX* AIS fields having exposure times larger than 90 s. In order to keep only good FIR data we discarded those galaxies for which the probability of a correct optical identification of the FIR-selected galaxies was lower than 50%, as listed in the PSCz. As for the NUV-selected sample, galaxies for which the cirrus parameter (as listed in the PSCz) was larger than 2 were discarded. A total of 163 galaxies were selected; all but two of them (Q00443+1038 and Q23367−0448) have published radial velocities. As galaxies were selected from the PSCz, the imposed limiting flux at 60 μm was 0.6 Jy. This limit, combined with the one estimated for the *GALEX* AIS at NUV ($\mathrm{AB_{NUV}} \sim 20.5$ mag; Morrissey et al. 2005), results in detections at NUV for all the galaxies with dust attenuation as large as ~ 4.4 mag (Buat et al. 2005). Indeed, only two galaxies (Q00443+1038 and Q00544+0347) were not detected in the NUV frames, and a total of 23 were not detected in the FUV frames.

The NUV and FUV photometry of the FIR-selected galaxies was performed using the same technique as for the NUV-selected galaxies.

2.3. Completeness and Bias of the Samples

Before drawing conclusions about the properties of the samples, we have to check on just how representative they are. Be-
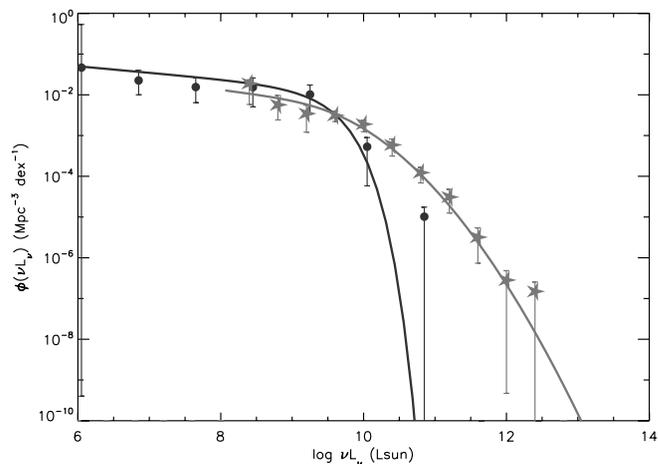

FIG. 1.—NUV (*circles*) and 60 μm (*stars*) LFs for the NUV- and FIR-selected samples. The lines connecting the circles and stars correspond to the NUV and 60 μm LFs from Wyder et al. (2005) and Takeuchi et al. (2003) respectively. Error bars correspond to 1 σ uncertainty. [*See the electronic edition of the Supplement for a color version of this figure.*]

cause of the reduced statistics of the samples, if the sampled volumes are not large enough it could be that some luminosity ranges are oversampled or undersampled with respect to reference samples defined over larger volumes of the local universe.

We check the representative nature of our samples by building LFs and comparing them to the standard ones at $z = 0$, constructed from larger samples of galaxies (NUV LF of Wyder et al. [2005] and 60 μm LF of Takeuchi et al. [2003]). We calculate both NUV and 60 μm LFs of our sample with the Lynden-Bell method (Lynden-Bell 1971), implemented to obtain the normalization using the formulation of Takeuchi et al. (2000). The calculation of the uncertainty is based on a bootstrap resampling method (Takeuchi et al. 2000). We note that the Lynden-Bell method is robust against density inhomogeneities, and hence we can trust the LF so determined (see Takeuchi et al. 2000 for details). The results are shown in Figure 1. The error bars correspond to 1 σ uncertainties. The agreement between the LFs of our samples and the corresponding LFs from larger samples is very good, so we are confident that in spite of their small size our samples are representative of flux-limited NUV and FIR samples in the local universe.

We also compare the volumes from which the samples were extracted. Figure 2*a* shows the redshift distributions for both samples. The median values are 0.013 and 0.027 for the NUV- and FIR-selected samples, respectively. At a first glance, this means that the FIR selection samples a volume 8 times larger than the corresponding NUV selection. However, we must recall that the redshift distribution of a flux-limited sample is strongly dependent on the shape of the LF, and as shown in Figure 1, the NUV and 60 μm LFs are very different. In Figure 2*b* we show the theoretical redshift distributions for NUV- and FIR-selected samples with the same limiting fluxes as our two samples. Details of the calculation are given in Appendix A. As can be seen, the theoretical median values of the redshift for both samples are consistent with the ones obtained from the observational data. A limiting magnitude of $\mathrm{AB_{NUV}} = 18$ mag is required to obtain similar median values of the redshift distributions of both samples, as we show in Figure 2*c*. And in this case, most of the galaxies detected in the NUV will not have any counterpart in the FIR. This behavior of the redshift distribution can be understood intuitively. Indeed, the flux density selection procedure omits intrinsically low-luminosity objects from the sample, whereas
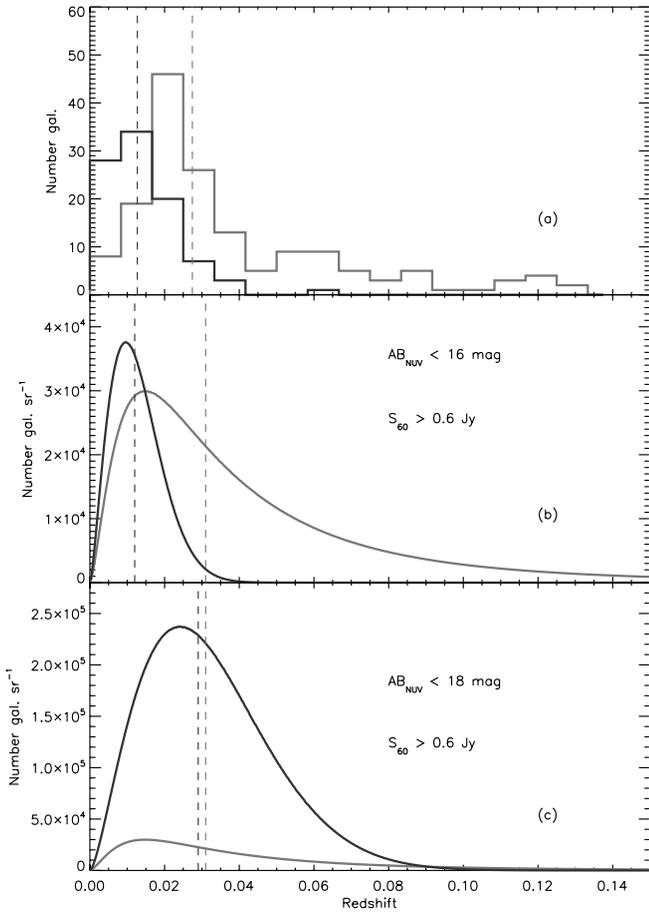
FIG. 2.—(*a*) Redshift distributions for the NUV (*darker histogram*) and FIR (*lighter histogram*) selected galaxies. (*b*) Theoretical redshift distributions for samples of galaxies with the same limiting fluxes as our samples. (*c*) Same as (*b*), but for an NUV-selected sample with $AB_{NUV} \leq 18$ mag. Vertical dashed lines in the three panels correspond to the median values of each distribution. [*See the electronic edition of the Supplement for a color version of this figure.*]

FIG. 3.—Plot of L_{60} vs. L_{NUV} (not corrected for attenuation) for the NUV (*circles*) and FIR (*stars*) selected samples. Arrows indicate upper limits. Dashed curves represent the loci of points with $L_{tot} = 10^7$, 10^8, 10^9, 10^{10}, and 10^{11} $L_{\odot}$, respectively. The dotted line corresponds to $L_{NUV} = L_{60}$. The lower dashed line corresponds to the maximum attenuation below which the FIR-selected sample is complete, and the upper dashed line corresponds to the minimum attenuation above which the NUV-selected sample is complete. The larger stars and circles correspond to the UVLGs of the FIR- and NUV-selected samples, respectively. [*See the electronic edition of the Supplement for a color version of this figure.*]

bright objects are hardly affected by the flux selection. To the degree that the LF is well reconstructed from the flux-limited/magnitude-limited samples, these samples can be said to be representative, with respect to luminosity and/or flux density, and it is indeed the case for the present work.

3. RELATION BETWEEN L_{60} AND L_{NUV}

The physical link between the FIR and UV luminosities of galaxies is rather complex. On one hand, both are related to the light of young stars, so one expects a correspondence between the two. On the other hand, the FIR emission is due to the absorption of the UV light, thereby leading to an anticorrelation. Since our samples were built to avoid upper limits—i.e., most of the galaxies selected in the NUV (or at 60 μm) are also detected at 60 μm (or in the NUV)—we are able to discuss statistically the intrinsic relation between the two wavelengths and to outline the specifics of NUV versus FIR selection effects.

In Figure 3 we plot L_{NUV} versus L_{60} for both samples.[13] The two samples exhibit very different behaviors: the NUV-selected galaxies show a good correlation between both luminosities, with a correlation coefficient (in log units) of $r \simeq 0.8$. Conversely, the
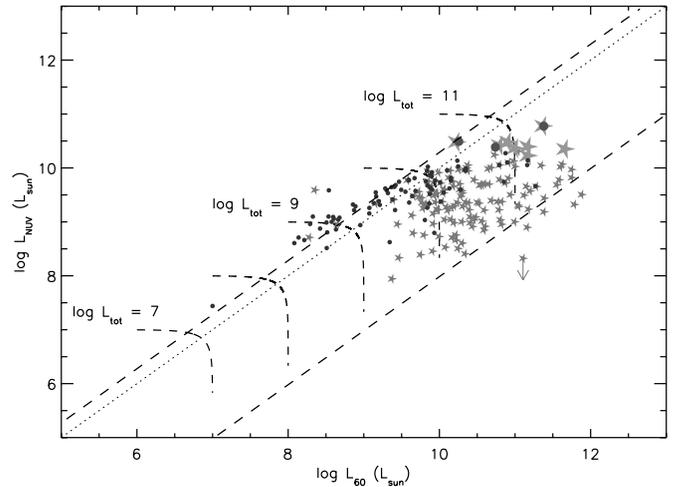
dispersion is very large for FIR-selected galaxies, and the correlation coefficient is low: $r \simeq 0.3$.

NUV-selected galaxies appear intrinsically less luminous at 60 μm than FIR-selected ones. This is also true for the sum of both luminosities, $L_{tot} = L_{NUV} + L_{60}$, which is supposed to be a crude estimate of the bolometric luminosity of galaxies related to recent star formation (e.g., Martin et al. 2005b). Although the luminosity distribution within each sample is the combined effect of the LFs and selection criteria, this result is confirmed by other studies and from the comparison of the 60 μm and NUV LFs themselves (e.g., Martin et al. 2005b; Buat et al. 2005). Both distributions flatten at higher luminosities, reflecting a general increase of the dust attenuation already pointed out in the literature by several authors (Wang & Heckman 1996; Buat et al. 1999; Sullivan et al. 2001; Vijh et al. 2003).

One could argue that the difference in luminosity between the two samples is a consequence of bias in the sampling. We show in Figure 3 the line corresponding to the lower limit of the NUV attenuation above which the NUV-selected sample is complete, and the line corresponding to the upper limit of the NUV attenuation below which the FIR-selected sample is complete. Thus, the fact that only very few low-luminosity and low-attenuation FIR-selected galaxies are detected must be taken as real. Low-luminosity, high-attenuation galaxies should have been detected by our FIR survey if they were present. For the same reason, very luminous galaxies should have been detected in the NUV survey if they existed.

The good correlation found between L_{NUV} and L_{60} for the NUV-selected galaxies has to be related to their rather low dust attenuation: in these galaxies both L_{NUV} and L_{60} represent a significant part of the total luminosity of the galaxies. This result holds for intrinsically faint galaxies ($L_{tot} \leq 2 \times 10^9$ $L_{\odot}$). The very loose correlation found for FIR-selected galaxies may also be explained by the effect of dust attenuation. With a mean dust attenuation larger than 2 mag, the NUV luminosity becomes a poor tracer of the galaxies' total luminosity, whereas the 60 μm luminosity is not very different from the bolometric emission of

---

[13] Throughout the paper the NUV and 60 μm luminosities L_{NUV} and L_{60} are calculated as νL_{ν} expressed in solar units. The adopted value for the bolometric solar luminosity is $L_{\odot} = 3.83 \times 10^{33}$ ergs s^{-1}.

TABLE 2
Basic Properties of the Sample Galaxies

Name (1)	UV Selected (2)	FIR Selected (3)	R.A. (J2000.0) (4)	Decl. (J2000.0) (5)	Velocity (km s^{-1}) (6)	Distance (Mpc) (7)	Type (8)	IRAS ID (9)
Mrk 544	Yes	No	00 04 48.70	−01 29 54.60	7110	101.39	S?	F00022−0146
NGC 10........................	Yes	Yes	00 08 34.56	−33 51 27.25	6811	94.62	Sbc	Q00060−3408
NGC 35........................	Yes	Yes	00 11 10.46	−12 01 14.74	5964	83.95	Sb	Q00086−1217
NGC 47........................	Yes	Yes	00 14 30.42	−07 10 06.28	5700	80.54	Sbc	Q00119−0726
NGC 101.......................	Yes	No	00 23 54.72	−32 32 09.06	3383	45.92	Sc	F00214−3248

Notes.—Units of right ascension are hours, minutes, and seconds, and units of declination are degrees, arcminutes, and arcseconds. Col. (1): Name. Col. (2): Flag indicating membership in the NUV-selected subsample. Col. (3): Flag indicating membership in the FIR-selected subsample. Cols. (4) and (5): Right ascension and declination. Col. (6): Heliocentric velocity. Col. (7): Distance derived from the velocity corrected for the Local Group infall into Virgo and $H_0 = 70$ km s^{-1} Mpc^{-1}. Col. (8): Morphological type from NED. Col. (9): IRAS identifier: F for FSC origin; Q, O, R for PSCz origin; SCANPI for absence in both catalogs. Table 2 is published in its entirety in the electronic edition of the Astrophysical Journal Supplement. A portion is shown here for guidance regarding its form and content.

the young stars. Some fluctuations in the percentage of NUV photons escaping the galaxies can induce large variations in the NUV observed luminosity on an absolute scale without any strong physical difference on the scale of the total luminosity of the galaxies.

We make a final comment on the so-called UV-luminous galaxies (UVLGs; defined as those with $L_{\rm FUV} \geq 2 \times 10^{10}\, L_\odot$ in Heckman et al. 2005). We found three ULVGs in our NUV-selected sample and a total of eight (including the previous three) in the FIR-selected sample. All but one of these galaxies are more luminous at 60 μm than in the NUV (in fact, most of them are luminous infrared galaxies [LIRGs]), and their attenuation is typically larger than 1 mag. This means that these galaxies are not only UV luminous but also very luminous from a bolometric point of view.

4. SELECTION EFFECTS ON OBSERVATIONAL QUANTITIES AND PHYSICAL PROPERTIES OF GALAXIES

The main aim of this section is to show the effect of the selection criteria of samples of galaxies on observational and physical quantities. We now show that the selection criteria of a sample of galaxies play an important role in defining the nature of the galaxies selected and, thus, in their averaged properties. Accordingly, we warn against the unqualified comparison of results obtained from samples of galaxies selected on the basis of different criteria.

In order to reduce the uncertainties associated with the FIR and NUV fluxes, we impose further constraints on our galaxy sample:

1. Elliptical galaxies, S0s, and active galactic nuclei (Seyfert galaxies and QSOs) were excluded since the origin of their 60 μm and NUV fluxes is clearly not associated with recent star formation. The necessary classification information is available for most of the NUV-selected galaxies, but this turned out not to be the case for the FIR-selected galaxies, so contamination of the sample by ellipticals and/or active galactic nuclei among these galaxies cannot be totally excluded. Galaxies with extraneous radio sources (from the NVSS and/or FIRST surveys) within the IRAS beam were also excluded since part of the FIR flux from these galaxies could be due to contaminating background objects.

2. Multiple galaxies, not resolved by the IRAS beam but clearly resolved into various components in the GALEX frames, were excluded, since a one-to-one 60 μm–NUV association is not possible for them.

After applying these criteria, we ended up with 59 and 116 galaxies from the original NUV- and FIR-selected samples, re-

spectively. Hereafter, we use these restricted subsamples for our analysis of star-formation-related properties, but we continue using the terminology "FIR- and NUV-selected samples" to refer to the restricted subsamples. Given that all the galaxies were extracted from the same region of the sky, some of them belong to both subsamples. Their basic properties are listed in Table 2.

Table 3 gives some useful photometric data for the galaxies in the restricted subsamples. For some galaxies, equations (1) and (2) gave negative values of the NUV and FUV attenuations, which is of course, unphysical. In fact, this is an artifact of the polynomial fitting used to derive a functional form for the attenuation in Buat et al. (2005). Throughout this paper these attenuations will be considered as zero. Given that the FIR fluxes were extracted from different catalogs (PSCz for the FIR-selected sample and FSC/SCANPI for the NUV-selected sample), for those galaxies belonging to both samples we list the FIR entries corresponding to the PSCz catalog. For those galaxies not present in the FSC and not detected by SCANPI at 60 μm, we list $f_{60} \leq 0.2$ Jy, which is the nominal limiting flux of the FSC. No estimate of an upper limit at 100 μm is given for these galaxies. For galaxies with no detection in 2MASS we adopt the limiting value of $H = 13.9$ mag (3 mJy), as published in Jarrett et al. (2000). In Table 4 we list some star formation properties that are used in our discussion below.

4.1. SFR Derivations

This section is devoted to a detailed comparison of the recent SFR as seen in the FIR- and NUV-selected samples. Although other estimators of the recent SFR can be found in the literature (see Kennicutt 1998 for an interesting review of several methods to derive the SFR), we focus on only two of them, those using the NUV and FIR fluxes. Our aim is to compare commonly used recipes to derive the SFR from the UV and FIR luminosity of the galaxies. Therefore we make very classical calculations, as described below. For consistency, we rederive the calibrations in a homogeneous way, adapted to the GALEX bands: the formulae are found to be very similar to those of Kennicutt (1998).

The underlying physical justification for deriving the SFR of a galaxy from the UV luminosity is the following: most of the UV photons emerging from a galaxy originate in the atmospheres of stars younger than $\sim 10^8$ yr. Thus, the SFR is proportional to the UV luminosity emitted by the young stars under the assumption that the SRF is approximately constant over this timescale. This is reasonable given that Salim et al. (2005) and Burgarella et al. (2005) found that the intensity of the youngest burst in large samples of nearby galaxies contributes typically less than 5% to the total. However, the presence of dust absorbs part of the UV

TABLE 3
PHOTOMETRIC PROPERTIES OF THE SAMPLE GALAXIES

Name (1)	AB_{NUV} (mag) (2)	AB_{FUV} (mag) (3)	f_{60} (Jy) (4)	f_{100} (Jy) (5)	H (mag) (6)	A_{NUV} (mag) (7)	A_{FUV} (mag) (8)
Mrk 544	15.75	15.97	0.49	1.11	12.50	0.71	0.96
NGC 10...................................	15.48	15.98	0.66	2.97	9.50	1.59	2.10
NGC 35...................................	15.55	15.89	1.31	2.34	11.91	1.29	1.67
NGC 47...................................	15.46	15.97	0.85	2.57	10.25	1.02	1.49
NGC 101.................................	14.78	14.98	0.55	1.75	10.74	0.50	0.72

NOTES.—Col. (1): Optical identifier. Col. (2): NUV magnitude corrected for Galactic extinction. Col. (3): FUV magnitude corrected for Galactic extinction. Col. (4): Flux density at 60 μm. Col. (5): Flux density at 100 μm. Col. (6): H magnitude from 2MASS Extended Source Catalog. For galaxies with no detection at 2MASS we adopt the limiting value of $H = 13.9$ mag (3 mJy) as given by Jarrett et al. (2000). Col. (7): NUV attenuation derived as indicated in Buat et al. (2005). Col. (8): FUV attenuation derived as indicated in Buat et al. (2005). Table 3 is published in its entirety in the electronic edition of the *Astrophysical Journal Supplement*. A portion is shown here for guidance regarding its form and content.

light escaping from galaxies and breaks down the proportionality between the SFR and the observed UV luminosity.

As star-forming galaxies may present a large variety of relative geometries between stars and dust, the scattering of the stellar photons through the interstellar medium may introduce a fraction of them in the line of sight before they escape the galaxy. Thus, the effect of the dust differs from a pure extinction but is a complex combination of absorption and scattering. Following Gordon et al. (1997) we use the term "dust attenuation" for this global process at work in galaxies. The most commonly accepted method to estimate the dust attenuation at UV wavelengths is to use the ratio of FIR to UV fluxes (Buat & Xu 1996; Meurer et al. 1999; Gordon et al. 2000). Several analytical expressions are already available in the literature for different UV wavelengths (Panuzzo et al. 2003; Kong et al. 2004; Buat et al. 2005). All these expressions are fairly consistent except at high values of the dust attenuation, where some dispersion appears (e.g., Meurer et al. [1999], Kong et al. [2004], and Buat et al. [2005] at $\lambda \sim 1500$ Å). In this work we use the prescription of Buat et al. (2005) to obtain the corrected NUV and FUV luminosities:

$$A_{NUV} = -0.0495x^3 + 0.4718x^2 + 0.8998x + 0.2269, \quad (1)$$

where $x = \log(L_{IR}/L_{NUV})$, and

$$A_{FUV} = -0.0333y^3 + 0.3522y^2 + 1.1960y + 0.4967, \quad (2)$$

where $y = \log(L_{IR}/L_{FUV})$.

Once the observed NUV and FUV luminosities have been corrected for dust attenuation, the SFRs can be derived using the expressions[14]

$$\log SFR_{NUV}(M_\odot \ yr^{-1}) = \log L_{NUV,corr}(L_\odot) - 9.33, \quad (3)$$

$$\log SFR_{FUV}(M_\odot \ yr^{-1}) = \log L_{FUV,corr}(L_\odot) - 9.51. \quad (4)$$

In Figure 4 we show the ratio SFR_{NUV}/SFR_{FUV} as a function of L_{tot} ($=L_{NUV} + L_{60}$), which traces the bolometric luminosity related to recent star formation and has the advantage of being a purely observational quantity. As this figure shows, both quantities are equivalent with a dispersion of about 20%. Since our sample is NUV-selected, hereafter we use the NUV as our reference wavelength for star-formation-related properties.

The luminosity at IR wavelengths provides a different avenue to the derivation of the SFR. Dust absorbs photons at UV wavelengths and re-emits most of them at IR wavelengths (8–1000 μm). Under the hypothesis that all the UV photons are absorbed by dust, the IR luminosity would be a direct tracer of the SFR of a galaxy. One source of uncertainty is the difficulty in estimating the total IR luminosity from the FIR flux at only one or two wavelengths. In this paper we use the prescription of Dale et al. (2001) and derive L_{IR} by using f_{60} and f_{100}. For the galaxies for which only f_{60} is available we use the mean value of f_{60}/f_{100}

[14] This formula has been derived from Starburst99 (Leitherer et al. 1999) and assuming solar metallicity and a Salpeter IMF from 0.1 to 100 $M_\odot$.

TABLE 4
STAR-FORMATION-RELATED PROPERTIES OF THE SAMPLE GALAXIES

Name (1)	log SFR_{NUV} (2)	log SFR_{FUV} (3)	log SFR_{dust} (4)	log SFR_{tot}(NUV) (5)	log SFR_{tot}(FUV) (6)	log $\langle SFR \rangle$ (7)
Mrk 544	0.83	0.85	0.60	0.80	0.75	0.81
NGC 10..................	1.23	1.24	1.07	1.09	1.02	1.95
NGC 35..................	0.98	1.00	0.78	0.84	0.79	0.88
NGC 47..................	0.87	0.86	0.78	0.85	0.77	1.51
NGC 101................	0.45	0.46	0.13	0.43	0.38	0.83

NOTES.—Col. (1): Identifier of the galaxy. Col. (2): SFR_{NUV} from eq. (3). Col. (3): SFR_{FUV} from eq. (4). Col. (4): SFR_{dust} from eq. (5). Col. (5): SFR_{tot}(NUV) from eq. (6). Col. (6): SFR_{tot}(FUV) from eq. (6) but using SFR_{FUV}^0 instead of SFR_{NUV}^0. Col. (7): $\langle SFR \rangle$ averaged over the galaxy's lifetime, estimated as indicated in Appendix B. SFRs are in units of $M_\odot$ yr^{-1}. Table 4 is published in its entirety in the electronic edition of the *Astrophysical Journal Supplement*. A portion is shown here for guidance regarding its form and content.
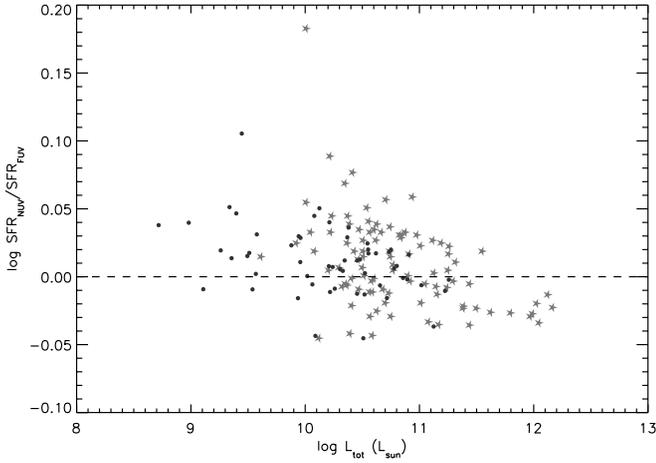
Fig. 4.—Plot of $\log(\mathrm{SFR_{NUV}/SFR_{FUV}})$ vs. $\log L_{\rm tot}$. Symbols are as in Fig. 3. [*See the electronic edition of the Supplement for a color version of this figure.*]

Fig. 5.—Plot of $\log(\mathrm{SFR_{NUV}/SFR_{dust}})$ vs. $\log L_{\rm tot}$. Symbols are as in Fig. 3. The right y-axis indicates the NUV dust attenuation. [*See the electronic edition of the Supplement for a color version of this figure.*]

estimated using the galaxies detected at both wavelengths. If we assume the same scenario as for equation (3), the SFR can be expressed as

$$\log \mathrm{SFR_{dust}}(M_\odot \ \mathrm{yr}^{-1}) = \log L_{\rm IR}(L_\odot) - 9.75. \qquad (5)$$

However, equation (5) is a good approximation only for the most extreme starbursts, since many of the FIR-selected galaxies are, in fact, detected at UV wavelengths. A further limitation of this method concerns the fraction of the total IR luminosity heated by old stars (the cirrus component, hereafter represented by η), which should be removed before applying equation (5). This quantity is known to depend on the morphological types of galaxies (Sauvage & Thuan 1992), but precise estimates for individual galaxies are subject to large uncertainties (Bell 2003).

The SFRs estimated from these methods are often compared in the literature for individual objects or for large samples of galaxies. In order to see whether these two methods are consistent with each other we show here a comparison of the two using the galaxies of our two samples. Figure 5 shows the ratio $\mathrm{SFR_{NUV}/SFR_{dust}}$ as a function of $L_{\rm tot}$; each sample shows a different behavior. For the NUV-selected sample (*circles*), $\mathrm{SFR_{NUV}}$ is always larger than $\mathrm{SFR_{dust}}$ (and the ratio can be as high as 3), but the discrepancy is lowered as $L_{\rm tot}$ (and $A_{\rm NUV}$) increase. This result is expected since we have seen in § 3 that low-luminosity galaxies are brighter in the NUV than at 60 μm. This affirms that $\mathrm{SFR_{dust}}$ cannot give a proper estimation of the SFR for these galaxies.

The FIR-selected galaxies extend the trend found for the NUV-selected sample to higher luminosities. For values of $L_{\rm tot} \geq 3 \times 10^{10}$ (and for higher values of the dust attenuation), where no NUV-selected galaxies are present, $\mathrm{SFR_{dust}}$ systematically exceeds $\mathrm{SFR_{NUV}}$ by a factor of $\sim$2. One reason that could play a role in this inconsistency between the two estimators is that the dust attenuation is not properly estimated for very dusty galaxies. In any case it does not make sense to use the corrected UV luminosity to measure the SFR for these IR-bright galaxies. In fact, Charmandaris et al. (2004) have reported decoupled IR and UV emissions for some dusty galaxies, which could be at the basis of the discrepancy found between $\mathrm{SFR_{NUV}}$ and $\mathrm{SFR_{dust}}$ found in this work for galaxies with large attenuation.

The conclusion of this analysis seems to be that $\mathrm{SFR_{NUV}}$ is a good tracer of the SFR for low values of attenuation, and in the opposite extreme $\mathrm{SFR_{dust}}$ must be used for very heavily attenuated galaxies. There is no obvious way to delimit these two
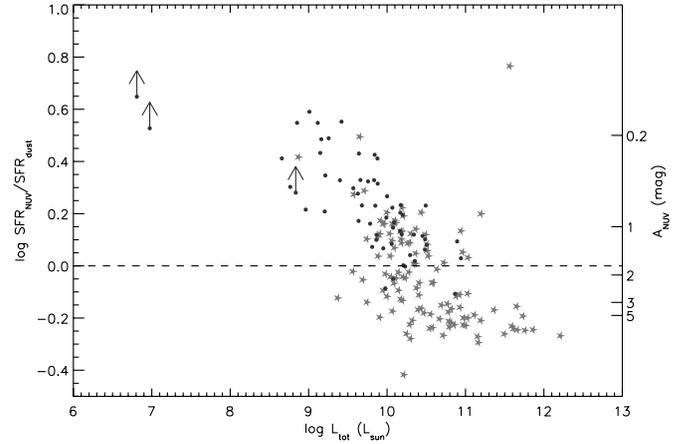
different regimes, or to chose which and which of the two indicators should be used in the intermediate cases. And so we warn users about any undiscriminated comparison of $\mathrm{SFR_{NUV}}$ and $\mathrm{SFR_{dust}}$ for samples of galaxies selected with different criteria.

An alternative tracer of the SFR containing information from NUV and IR luminosities has already been discussed in the literature (Hirashita et al. 2003; Iglesias-Páramo et al. 2004; Bell 2003):

$$\mathrm{SFR_{tot}} = \mathrm{SFR_{NUV}^0} + (1 - \eta)\mathrm{SFR_{dust}}, \qquad (6)$$

where η accounts for the IR cirrus emission and $\mathrm{SFR_{NUV}^0}$ is obtained following equation (3) but using $L_{\rm NUV,obs}$ (that is the observed NUV luminosity) instead of $L_{\rm NUV,corr}$. This estimator has the advantages of being free of the model dependence of the attenuation correction and containing information on the observed NUV and IR luminosities.

One limitation of this estimator, η, is the adopted value of the IR cirrus contribution. Hirashita et al. (2003) and Iglesias-Páramo et al. (2004) reported a value of $\eta \sim 0.4$ for normal disk galaxies. Accurate values of η for individual galaxies are not easily obtained, and instead, averaged values are often used. However, this parameter is strongly dependent on the sample of galaxies under study and cannot be easily generalized. Whereas an average value of $\eta \sim 0.4$ seems to apply for normal disk galaxies, a value of $\eta \sim 0$ seems to better represent the properties of starbursts (Hirashita et al. 2003). Bell (2003) also proposed a cirrus correction for a compilation of galaxies from the literature with FUV, optical, IR, and radio luminosities. He found $\eta \sim 0.32 \pm 0.16$ for galaxies with $L_{\rm IR} \leq 10^{11} \ L_\odot$ and $\eta \sim 0.09 \pm 0.05$ for galaxies with $L_{\rm IR} > 10^{11} \ L_\odot$. For our NUV-selected sample (similar to the normal star-forming galaxies of Hirashita et al.), a value of $\eta \sim 0.2$ gives similar values for $\mathrm{SFR_{NUV}}$ and $\mathrm{SFR_{tot}}(\mathrm{NUV})$. Although our NUV-selected sample must contain galaxies more active than that of Hirashita et al. (since their selection is based on optical fluxes rather than on UV fluxes), this result gives an idea of the uncertainties related to the determination of η. For practical issues, throughout this paper we use the value of η of Bell (2003)—not far from that of Hirashita et al. (2003)—when computing $\mathrm{SFR_{tot}}$, but keeping in mind that the uncertainties reported by this author are on the order of 50%.

Another limitation of $\mathrm{SFR_{tot}}$ is that it depends on the wavelength at which we measure the UV flux. In order to illustrate this point, we show in Figure 6 the ratio of $\mathrm{SFR_{tot}}(\mathrm{NUV})/\mathrm{SFR_{tot}}(\mathrm{FUV})$ as a function of $\mathrm{SFR_{tot}}(\mathrm{NUV})$ for both samples. As can be seen, for
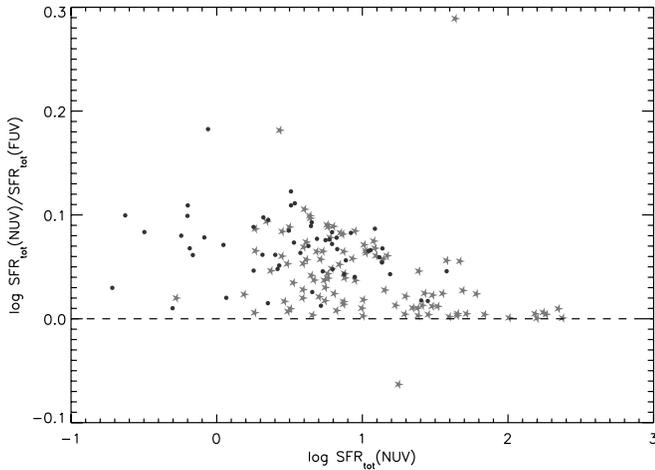
FIG. 6.—Plot of log [SFR$_{tot}$(NUV)/SFR$_{tot}$(FUV)] vs. log SFR$_{tot}$(NUV). Symbols are as in Fig. 3. [*See the electronic edition of the Supplement for a color version of this figure.*]

FIG. 7.—(*a*) Plot of log[SFR$_{NUV}$/SFR$_{tot}$(NUV)] vs. log SFR$_{tot}$(NUV). (*b*) Plot of log[SFR$_{dust}$/SFR$_{tot}$(NUV)] vs. log SFR$_{tot}$(NUV). Symbols are as in Fig. 3. [*See the electronic edition of the Supplement for a color version of this figure.*]

the NUV-selected galaxies SFR$_{tot}$(NUV) is systematically larger than SFR$_{tot}$(FUV) by about 20%. This discordance for the NUV-selected galaxies is due to the fact that the UV attenuation is not gray: $A_{NUV} \leq A_{FUV}$ for most galaxies (see Buat et al. [2005] and Table 3), and since we showed in Figure 4 that SFR$_{NUV} \approx$ SFR$_{FUV}$, it is obvious that SFR$_{NUV}^0 \geq$ SFR$_{FUV}^0$. On the contrary, for the brightest FIR-selected galaxies the agreement between SFR$_{tot}$(NUV) and SFR$_{tot}$(FUV) is good since for these galaxies SFR$_{tot}$ is dominated by SFR$_{dust}$. We conclude that SFR$_{tot}$ is stable to within 20% for whatever UV wavelength we measure the UV flux at.

We compare now SFR$_{tot}$(NUV) to the classical estimators SFR$_{NUV}$ and SFR$_{dust}$, in order to set their domain of applicability. Figure 7a shows the comparison between SFR$_{NUV}$ and SFR$_{tot}$. At low values of the SFR both quantities are almost identical for the NUV-selected galaxies. This is expected since for these galaxies both A_{NUV} and L_{IR} are almost negligible and SFR$_{NUV} \approx$ SFR$_{NUV}^0$. As the SFR grows, we note an increase of SFR$_{NUV}$ with respect to SFR$_{tot}$, but always within ∼15%. This increase could be due to the choice for the cirrus correction and/or to the fact that A_{NUV} does not exactly correspond to the dust emission (since factors other than absorption do play a role in the attenuation, such as, for example, the relative geometry between stars and dust). Finally, the NUV-selected galaxies with the largest values of SFR show a decrease of SFR$_{NUV}$ with respect to SFR$_{tot}$. We stress that these galaxies have $L_{IR} > 10^{11} L_{\odot}$ and so their cirrus correction is different from the rest. All in all we find that for the NUV-selected galaxies, basically those with SFR$_{NUV} \leq 15 M_{\odot}$ yr^{-1}, SFR$_{NUV}$ and SFR$_{tot}$ are equivalent to within ∼15%. The FIR-selected galaxies show a different behavior. Whereas those with $L_{IR} < 10^{11} L_{\odot}$ show a ∼15% excess of SFR$_{NUV}$ with respect to SFR$_{tot}$, similar to the NUV-selected galaxies, for those with $L_{IR} > 10^{11} L_{\odot}$, SFR$_{NUV}$ is well below SFR$_{tot}$. This is easily understood as a consequence of the already mentioned discrepancy between SFR$_{dust}$ and SFR$_{NUV}$ for galaxies dominated by their IR emission.

In Figure 7b we compare SFR$_{dust}$ and SFR$_{tot}$. The NUV-selected galaxies follow a very dispersed trend with SFR$_{dust}$/SFR$_{tot}$ increasing with SFR$_{tot}$. This behavior is due to the fact that SFR$_{dust}$ lacks the UV contribution that is dominant in these galaxies. The FIR-selected galaxies obey two different trends: for galaxies with SFR$_{tot} \leq 15 M_{\odot}$ yr^{-1}, the ratio log SFR$_{dust}$/SFR$_{tot} \sim 0$, although with a dispersion of ∼0.2 dex. This large dispersion is due to the

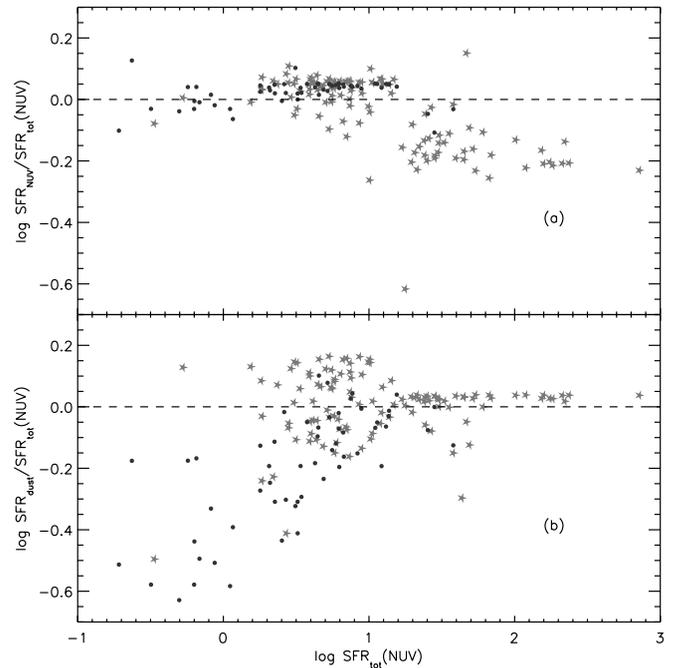contribution of the NUV luminosity to SFR$_{tot}$, which is important for the less attenuated galaxies. On the contrary, at large values of SFR$_{tot}$ the average value of log SFR$_{dust}$/SFR$_{tot} \sim$ 0.04 dex with a very small dispersion. This is a consequence of the fact that most of these galaxies have $L_{IR} > 10^{11}$ and are dominated by their IR emission, so the difference between SFR$_{dust}$ and SFR$_{tot}$ corresponds basically to the cirrus correction applied to SFR$_{tot}$, which is minimal.

Bell (2003) proposed a calibration of the SFR similar to the one described in equation (6) but using FUV as the reference UV wavelength. His method is based on the relation he found between L_{IR}/L_{FUV} and L_{IR} [$L_{IR}/L_{FUV} \sim (L_{IR}/10^9)^{1/2}$] for a compilation of galaxies from the literature with FUV, optical, IR, and radio luminosities. One can see in Figure 8 that our NUV-selected galaxies follow Bell's relation well, whereas this is not the case
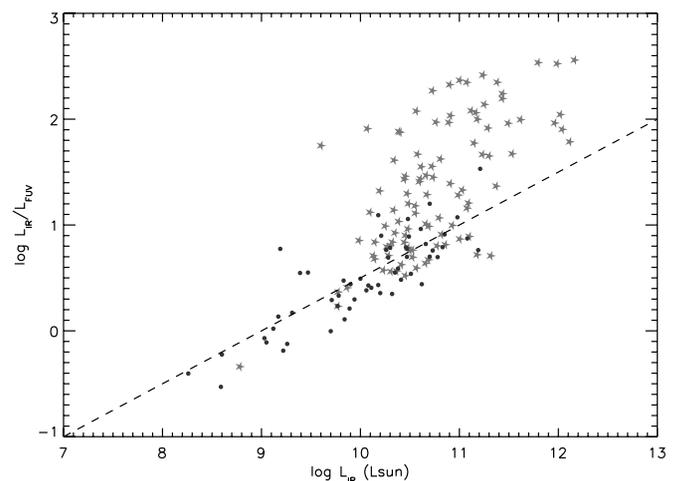

FIG. 8.—Plot of L_{IR} vs. L_{IR}/L_{FUV}. Symbols are as in Fig. 3. The dashed line corresponds to the relation $L_{IR}/L_{FUV} \sim (L_{IR}/10^9)^{1/2}$ of Bell (2003). [*See electronic edition of the Supplement for a color version of this figure.*]
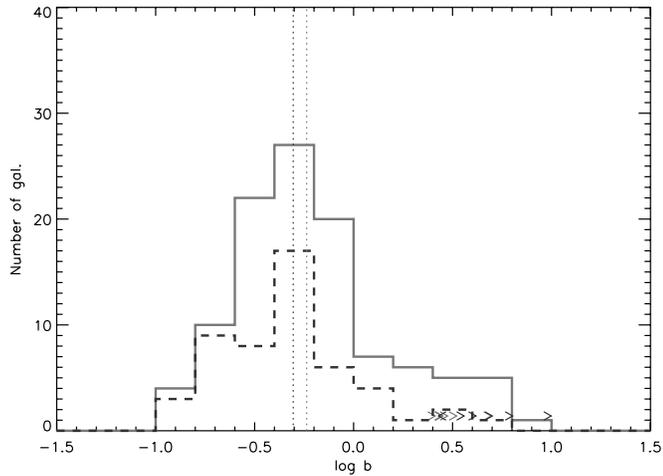
for the FIR-selected sample. The galaxy sample used by Bell is therefore closer to a UV selection than to an IR one. Again we emphasize the importance of the selection biases in deriving SFRs.

The overall conclusion emerging from this study is that SFR_{tot} seems to be a proper estimator of the SFR of galaxies whatever their dust content is, since it avoids the main problems of the classical estimators SFR_{NUV} and SFR_{dust} and is consistent with them within their respective domains of applicability to within $\sim 15\%$. We again warn against indiscriminate comparisons of the SFRs of galaxies estimated with these classical estimators since the results could be strongly affected by selection biases, as we have illustrated in this section. The combined uncertainty of SFR_{tot} due to the choice of the UV wavelength at which we measure the UV flux and to the cirrus contribution to the IR luminosity is $\lesssim 55\%$. Throughout this paper, we adopt $SFR_{tot}(NUV)$ as our proxy to trace the recent SFR.

4.2. *Star Formation History*

The determination of the SFR of a galaxy gives information about the total number of young stars that are being formed. But this does not necessarily mean that the light coming from this galaxy is dominated by these young stars, given that most galaxies are composed of a mixture of various stellar populations of different ages. This parameter is of major importance in understanding the SFH of the universe. Recent results based on large amounts of SDSS data suggest that the higher the mass of a galaxy, the earlier its stars were formed (Heavens et al. 2004), thus supporting the so-called downsizing explanation for the SFH of galaxies already proposed by several authors (e.g., Cowie et al. 1996; Brinchmann & Ellis 2000; Boselli et al. 2001). We devote this section to the study of the SFH of the galaxies in our samples.

A quantitative estimation of the SFH of a galaxy requires information relating the relative contributions of young and old stars. The birthrate parameter (hereafter b) has been proposed as a quantitative estimator of the recent SFH of a galaxy (Scalo 1986). It is defined as the ratio between the current and the past-averaged SFR:
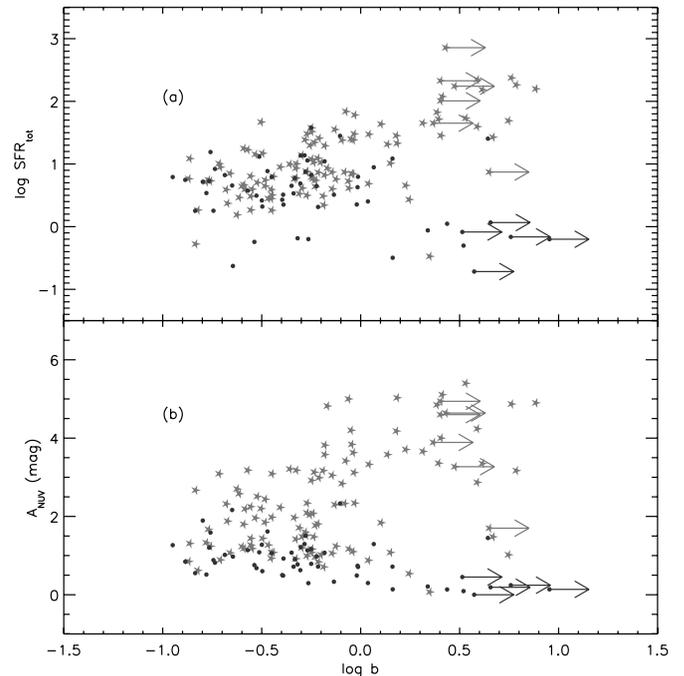
$$b = \frac{SFR}{\langle SFR \rangle}. \tag{7}$$

Since b depends on the overall SFH of the galaxy, an accurate estimation from observational quantities is complex and involves several approximations. A detailed derivation of b following the prescriptions of Boselli et al. (2001) can be found in Appendix B. As explained in § 4.1, the NUV luminosity is sensitive to the SFR over a timescale of $\sim 10^8$ yr, and thus b is not sensitive to shorter timescale variations in the SFH. However, this is not a serious problem since Burgarella et al. (2005) have shown that less than 20% of the galaxies in either sample have bursts younger than 10^8 yr.

Figure 9 shows the distributions of b for both samples of galaxies. The median values of both distributions are similar: 0.50 and 0.58 for the NUV- and FIR-selected galaxies, respectively. In Figure 10*a* we show the relation between SFR_{tot} and b for both samples. In the range of overlap between the two samples (approximately $0.5 \leq \log SFR_{tot} \leq 1.5$) the values of b are consistent, but beyond this region two different trends are seen: the NUV-selected galaxies show no trend of b with the SFR, whereas the FIR-selected galaxies show an increase of b for high SFR. This bimodal behavior of b is also seen in Figure 10*b*, where b is plotted as a function of the attenuation. Again, for the NUV-selected galaxies b increases at lower values of the attenuation, although this trend is very dispersed. The opposite holds for the FIR-selected galaxies, with galaxies with high b being the most attenuated. Thus, the picture emerging from this study is that galaxies dominated by young stellar populations fall into two categories: those showing low SFRs and low attenuation, which naturally appear in UV surveys, and those with high SFRs and large attenuation, mainly detected in FIR surveys.

4.3. *The Link between the H Luminosity and Star Formation Properties of Galaxies*

The baryonic mass of galaxies is a key parameter in understanding their evolution. It has been proposed as the parameter which governs the SFH, rather than the morphological type, for
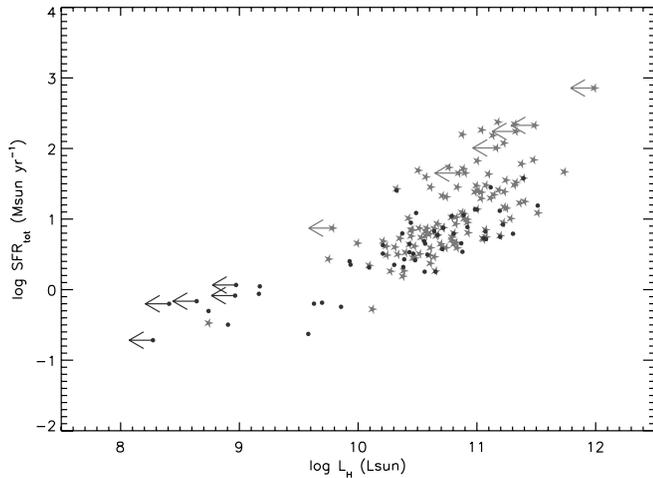
FIG. 11.—*H*-band luminosity vs. SFR$_{tot}$. Symbols are as in Fig. 3. [*See the electronic edition of the Supplement for a color version of this figure.*]

FIG. 12.—*H*-band luminosity vs. A_{NUV}. Symbols are as in Fig. 3. [*See the electronic edition of the Supplement for a color version of this figure.*]

example (Boselli et al. 2001). In addition, it is often used to derive some properties such as the dust attenuation in semiempirical models of formation and evolution of galaxies. For this reason we devote this section to a discussion of the effects of the sample selection on the relation between the mass and the star-formation-related properties of galaxies. As explained in the previous section, we use the *H*-band luminosity as a tracer of the galaxy mass.

First we show in Figure 11 SFR$_{tot}$ as a function of the *H*-band luminosity. Both samples show a positive relation between these two quantities, which means that more massive galaxies are also currently forming more young stars. This result is expected since we are comparing two extensive quantities. However, whereas the relation followed by the NUV-selected galaxies shows a small dispersion, the FIR-selected galaxies exhibit a more dispersed relation, especially at the most massive end. At high galaxian masses the range in SFR spans almost 2 orders of magnitude, which is not seen in the NUV-selected sample.

In Figure 12 we show the dust attenuation as a function of the *H*-band luminosity. Two different trends are seen in this plot. The NUV-selected galaxies show a fairly good correlation between the two quantities, with the dispersion increasing toward high *H*-band luminosities. On the contrary, the FIR-selected galaxies span an interval of almost 5 mag in dust attenuation and no correlation at all is shown with the galaxian mass. While the trend followed by the NUV-selected galaxies could be interpreted as a result of the mass-metallicity relation reported for samples of spiral and irregular galaxies (Garnet & Shields 1987; Zaritsky 1993) in the sense that more metallic galaxies contain more dust, there is no simple explanation for the lack of any trend shown by the FIR-selected galaxies.

Finally, we show in Figure 13 the *b*-parameter as a function of the *H*-band luminosity. The NUV-selected galaxies follow the classical trend that low-luminosity galaxies have larger values of *b* (e.g., Boselli et al. 2001). Some of the FIR-selected galaxies also follow this trend, although about 20% of them show large masses and large values of *b*. As shown in Figure 12, these galaxies are among the most attenuated of the FIR-selected sample. Overall, our galaxies are shifted toward higher values of *b* with respect to the sample of galaxies of Boselli et al. (2001). These authors adopt a slightly different IMF than we do ($M_{up} = 80\,M_{\odot}$ against $100\,M_{\odot}$) and different evolutionary synthesis codes. Nevertheless, the large shift in *b* found between the samples can probably
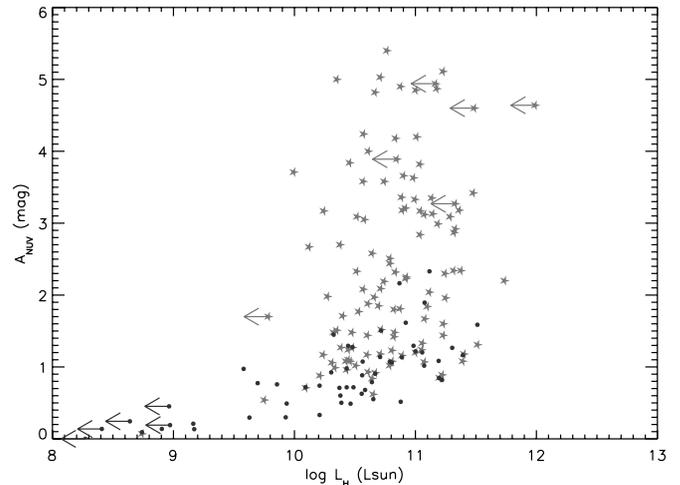
not be explained by these differences alone. The correction for dust attenuation could also partially explain the shift in *b*, since Boselli et al. assume average values of 0.20 mag for Sds and later types, and 0.60 mag for types earlier than Sd. For our NUV- and FIR-selected samples, the values of the dust attenuation estimated from the FIR/UV flux ratio of each of the individual galaxies show higher averaged values for the two categories of morphologies than those of Boselli et al., which would imply higher SFRs. However, this effect is diluted by the fact that for many objects in their sample, Boselli et al. estimate the SFR as the mean value of SFR$_{H\alpha}$ and SFR$_{UV}$. A further factor that could be responsible for the shift in *b* is the different selection effect of the sample: the sample of Boselli et al. (2001) is drawn from the nearby clusters Virgo, Cancer, Coma, and A1367 and from the Coma-A1367 super-cluster. Although a unique selection criterion was not applied, this sample can be defined as an optically selected sample of galaxies with a normal H I content. Thus, in their sample there is a nonnegligible fraction of Sa–Sab, bulge-dominated galaxies, which tend to lower the average value of *b* (see their Fig. 2). Since our selections are based on NUV and FIR fluxes, we argue that we are surely avoiding these kind of objects. Anyway, one
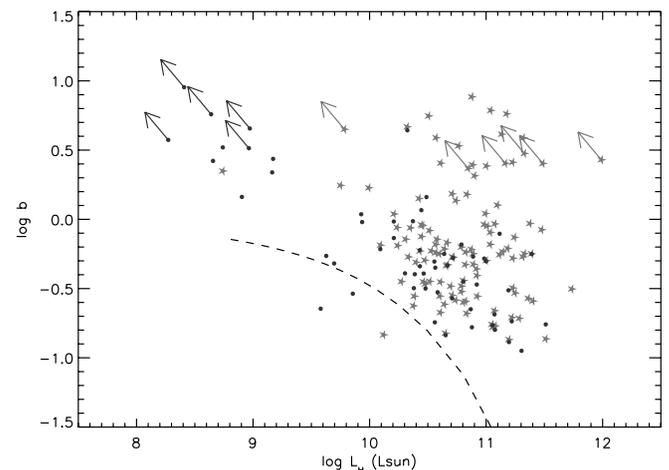

FIG. 13.—*H*-band luminosity vs. *b*. Symbols are as in Fig. 3. The dashed line corresponds to the calibration of Boselli et al. (2001) for their sample of late-type galaxies from nearby clusters with a normal H I content. [*See the electronic edition of the Supplement for a color version of this figure.*]

important point is that the NUV-selected galaxies follow the same relation between mass and b as the optically selected ones (disregarding the absolute calibration of both quantities) and that a fraction of the FIR-selected galaxies do not follow this trend.

We have seen that the relation of the star-formation-related properties with the mass of galaxies strongly depends on the selection procedure of the sample: whereas for NUV-selected galaxies low-luminosity galaxies are also of low mass, show low attenuation, and have high values of b, a selection based on the FIR fluxes yields a different result: a population having high attenuation, high mass, and strong star formation activity appears. This population is absent in the NUV-selected sample. Since these galaxies present very high values of attenuation (most of them are LIRGs and/or ULIRGs [ultraluminous infrared galaxies]), their UV (and optical) fluxes are strongly dimmed and for this reason they are often excluded from flux-limited surveys. However, even if these galaxies show such extreme properties, they do not put into question the downsizing picture for the SFH of galaxies since their contribution to the local cosmic SFR density is very low (see Takeuchi et al. 2005).

5. THE LOCAL COSMIC STAR FORMATION RATE DENSITY FROM DIFFERENT ESTIMATORS

We saw in § 4.1 that a proper estimation of the SFR is not possible with information restricted only to either NUV or FIR fluxes. However, big surveys usually provide large amounts of data only at single wavelengths, and thus an estimation of the density of the SFR over cosmological volumes has to be carried out under these constraints. The accuracy of the cosmic density of the SFR has already been discussed by Hirashita et al. (2003) using UV data from the FOCA balloon-borne imaging telescope. In this section we make a similar analysis using the new *GALEX* data.

The usual way to estimate the average SFR density is to construct the monochromatic LF and then to weight the corresponding contribution to the SFR at a given luminosity with the probability of finding a galaxy with this luminosity:

$$\rho_\lambda = \kappa_\lambda \int L_\lambda \phi(L_\lambda)\, dL_\lambda, \qquad (8)$$

where ρ_λ is the SFR density estimated from the flux at a given λ, κ_λ is the conversion factor between SFR_λ and L_λ, and $\phi(L_\lambda)$ is the LF.

A simple calculation using equations (3) and (8) and the NUV LF of Wyder et al. (2005) yields a value of $\rho_{NUV} = 0.009^{+0.007}_{-0.004}\ M_\odot$ $yr^{-1}\ Mpc^{-3}$ for the local cosmic SFR density. Unfortunately, there is not a simple relation linking the observed NUV luminosity and the attenuation (see Fig. 3 of Buat et al. 2005), so we adopt the median attenuation of our NUV-selected sample, which is $A_{NUV} = 0.78$ mag. After correcting for this median attenuation we obtain $\rho_{NUV,corr} = 0.018^{+0.013}_{-0.008}\ M_\odot\ yr^{-1}\ Mpc^{-3}$.

Takeuchi et al. (2005) report a value of the local cosmic star formation density derived from L_{IR} of $\rho_{IR} = 0.013^{+0.008}_{-0.005}\ M_\odot\ yr^{-1}$ Mpc^{-3}. However, we recall that this quantity does not account for the fraction of UV escaping photons or for the cirrus IR heating. For our FIR-selected sample, the median contribution of the NUV escaping luminosity to SFR_{tot} is 17%, which leads to $\rho'_{IR} = 0.016^{+0.010}_{-0.006}\ yr^{-1}\ Mpc^{-3}$. After correcting for the cirrus contribution assuming $\eta = 0.32$, we obtain $\rho_{IR,corr} = 0.011^{+0.007}_{-0.004}\ M_\odot$ $yr^{-1}\ Mpc^{-3}$, which is well below $\rho_{NUV,corr}$, although still within the 1 σ uncertainty. Although we have previously accepted that a cirrus correction of $\eta = 0.32$ is valid for galaxies with $L_{IR} \leq$

$10^{11}\ L_\odot$, and $\eta = 0.09$ for brighter galaxies, we argue that adopting just $\eta = 0.32$ for all the galaxies is not a bad approximation for this calculation since it can be seen in Takeuchi et al. (2005) that the contribution of $L_{IR}\phi(L_{IR})$ to the total $\int L_{IR}\phi(L_{IR})\, dL_{IR}$ of galaxies with $L_{IR} > 10^{11}\ L_\odot$ is very low and can hardly affect our calculations.

Proceeding analogously to § 4.1, we can add both contributions to get the total cosmic SFR, and we get $\rho_{tot} = \rho_{NUV} + (1 - \eta)\rho_{IR}\ (=0.009 + 0.009) = 0.018\ M_\odot\ yr^{-1}\ Mpc^{-3}$, which is in good agreement with $\rho_{NUV,corr}$, which means that correcting ρ_{NUV} with a median attenuation is a good approximation. We also stress that the NUV and IR contributions to ρ_{tot} are almost equal.

The discrepancy found with ρ_{IR} alone may be due to the average corrections applied. In order to obtain a better agreement between $\rho_{NUV,corr}$, ρ_{tot}, and $\rho_{IR,corr}$, two points should be studied in more detail:

1. A detailed knowledge of the cirrus component is required since this contribution is probably multivalued for a given value of L_{IR}. Although the morphological type seems to drive this parameter (Sauvage & Thuan 1992), it could also be dependent on b since this parameter also measures the relative weight of the young and old stellar populations. A more detailed study of a large samples of galaxies, covering a wide range of galaxian properties, could shed light on its fractional contribution to the total cosmic L_{IR} density.

2. The bivariate LF $\phi(L_{NUV}, L_{IR})$ appears to be the best way to estimate the fraction of UV photons escaping from the galaxy, which is required to correct ρ_{IR}. It is also required since for large values of L_{NUV}, the attenuation can take on multiple values, and thus an average value, such as the one used in this work, might be not the most appropriate.

Under these conditions, the cosmic SFR densities would be expressed as

$$\rho_{NUV,corr} = \int\int \kappa_{NUV} L_{NUV} \times 10^{A_{NUV}(L_{NUV},\, L_{IR})/2.5}$$
$$\times \phi(L_{NUV}, L_{IR})\, dL_{NUV}\, dL_{IR} \qquad (9)$$

and

$$\rho_{IR,corr} = \int\int \kappa_{IR}[1 - \eta(L_{IR},\, L_{NUV})]L_{IR}\left(1 + \frac{\kappa_{NUV}}{\kappa_{IR}}\frac{L_{NUV}}{L_{IR}}\right)$$
$$\times \phi(L_{NUV},\, L_{IR})\, dL_{NUV}\, dL_{IR}, \qquad (10)$$

or if we use the approximation of equation (6),

$$\rho_{tot} = \int\int \{\kappa_{IR}[1 - \eta(L_{IR},\, L_{NUV})]L_{IR} + \kappa_{NUV} L_{NUV}\}$$
$$\times \phi(L_{NUV},\, L_{IR})\, dL_{NUV}\, dL_{IR}. \qquad (11)$$

6. CONCLUSIONS

We have performed a detailed study of the star formation properties of two samples of galaxies selected on the basis of their NUV and FIR fluxes, which were found to be representative of the nearby universe when compared to samples drawn from larger volumes. The main conclusions of this work are as follows:

1. L_{NUV} and L_{60} are tightly correlated for the NUV-selected galaxies. The opposite holds for FIR-selected galaxies, which span a large range of L_{60} for a given value of L_{NUV} and show

larger values of attenuation. Intrinsically bright galaxies are more luminous at FIR than at NUV wavelengths, including the UV luminous galaxies (UVLGs), and they show moderate to high attenuation.

2. The SFRs deduced from the NUV fluxes, corrected for the dust attenuation (SFR_{NUV}), are not found to be consistent with those calculated using the total dust emission (SFR_{dust}). Whereas SFR_{NUV} is larger than SFR_{dust} for galaxies with low attenuation ($A_{NUV} \lesssim 1$ mag), the inverse is found for bright but highly extinguished galaxies, mostly selected in the IR: SFR_{NUV} is likely to underestimate the actual SFR in these galaxies by a factor of ~ 2. A combined estimator based on UV and IR luminosities with a cirrus correction depending on the IR luminosity seems to be the best proxy over the whole range of values of SFR. As a practical recipe we found that SFR_{tot} and SFR_{NUV} yield similar results for $SFR_{tot} \lesssim 15\ M_\odot\ yr^{-1}$, whereas SFR_{tot} and SFR_{dust} are almost equivalent for $SFR_{tot} \gtrsim 15\ M_\odot\ yr^{-1}$.

3. NUV-selected galaxies follow a trend whereby low-mass galaxies show lower SFRs, low attenuation, and higher values of b, indicating the existence of a dominant young stellar population. On the other hand, about 20% of the FIR-selected sample show high attenuation, high SFRs, and large values of b, most of them being LIRGs and/or ULIRGs. In spite of their discordant properties, these galaxies are not sufficiently abundant in the local universe to question the downsizing picture for the SFH seen at $z = 0$ from optical surveys.

4. The cosmic SFR densities of the local universe, estimated from the NUV and IR luminosities, are consistent to within 1 σ, although the difference between the two values is large, when average corrections for the attenuation, UV escaping photons, and IR cirrus component are applied. The sum of the individual contributions is quite consistent with the value obtained from the NUV luminosities corrected for average attenuation. A better knowledge of the cirrus contribution to L_{IR} and of the bivariate LF is required in order to better understand the large differences found between the monochromatic estimators of the local SFR density.

APPENDIX A

RELATION OF THE MEAN REDSHIFT OF GALAXIES AND THE LUMINOSITY FUNCTION: REPRESENTATIVITY OF SURVEY DEPTH

We show the strong dependence of the mean redshift on the shape of the LF. This means that the mean distance of galaxies does not represent the depth of a survey, but rather reflects an intrinsic property of the sample.

Since we treat a local sample of galaxies, we first approximate their distance by the classical Hubble law:

$$cz \simeq \frac{r}{H_0}, \tag{A1}$$

where c is the velocity of light and r represents the distance. We define $\mathcal{N}$ to be the surface density of galaxies on the sky, and denote the LF as an explicit function of the characteristic luminosity L_* as $\phi(L/L_*)$. Then, $\mathcal{N}$ is written as (Peebles 1993, p. 119)

$$\mathcal{N} = \int \int \phi\left[\frac{L(r)}{L_*}\right] \frac{dL(r)}{L_*} r^2\, dr. \tag{A2}$$

Using the detected flux density S, this can be expressed as

$$\mathcal{N} = \int \int \phi\left[\frac{4\pi}{L_*}\left(\frac{c}{H_0}\right)^2 z^2 S\right] \frac{4\pi}{L_*}\left(\frac{c}{H_0}\right)^2 z^2\, dS \left(\frac{c}{H_0}\right)^3 z^2\, dz = \int \int \phi\left[\frac{4\pi}{L_*}\left(\frac{c}{H_0}\right)^2 z^2 S\right] \frac{4\pi}{L_*}\left(\frac{c}{H_0}\right)^5 z^4\, dS\, dz. \tag{A3}$$

We observe the distribution function of the sources with a *fixed* flux density S as

$$\frac{d^2\mathcal{N}}{dz\, dS} = \phi(\alpha z^2 S)\alpha\left(\frac{c}{H_0}\right)^3 z^4, \tag{A4}$$

where

$$\alpha \equiv \frac{4\pi}{L_*}\left(\frac{c}{H_0}\right)^2. \tag{A5}$$

The mean redshift of a flux-limited survey (limiting flux density S), $\langle z \rangle_{>S}$, is then defined as[15]

$$\langle z \rangle_{>S} \equiv \frac{\int_S^\infty \int_0^\infty [d^2\mathcal{N}/(dz\,dS')]z\,dz\,dS'}{\int_S^\infty \int_0^\infty [d^2\mathcal{N}/(dz\,dS')]\,dz\,dS'}. \tag{A6}$$

The numerator is obtained as

$$\int_S^\infty \int \frac{d^2\mathcal{N}}{dz\,dS'} z\,dz\,dS' = \frac{1}{2\alpha^2}\left(\frac{c}{H_0}\right)^3 \left[\int_0^\infty \phi(x)x^2\,dx\right]\int_S^\infty S'^{-3}\,dS' = \frac{1}{2\alpha^2}\left(\frac{c}{H_0}\right)^3 \left[\int_0^\infty \phi(x)x^2\,dx\right]\frac{S^{-2}}{2}. \tag{A7}$$

Here $x \equiv \alpha z^2 S'$, a luminosity normalized by the characteristic luminosity of the LF, L_*, and expressed in terms of flux density S'. Since the luminosity must be positive, the lower bound on the integration with respect to x is 0 and upper bound is large, effectively taken to be $+\infty$. Similarly, the denominator becomes

$$\int_S^\infty \int_0^\infty \frac{d^2\mathcal{N}}{dz\,dS'}\,dz\,dS' = \frac{1}{2\alpha^{3/2}}\left(\frac{c}{H_0}\right)^3 \left[\int_0^\infty \phi(x)x^{3/2}\,dx\right]\int_S^\infty S'^{-5/2}\,dS' = \frac{1}{2\alpha^2}\left(\frac{c}{H_0}\right)^3 \left[\int_0^\infty \phi(x)x^2\,dx\right]\frac{2S^{-3/2}}{3}. \tag{A8}$$

Both the numerator and the denominator of this part are the moment of the LF. This means that this is a function of its shape.

Combining equations (A6), (A7), and (A8), we have

$$\langle z \rangle_{>S} = 3\alpha^{-1/2} \frac{\int_0^\infty \phi(x)x^2\,dx}{\int_0^\infty \phi(x)x^{3/2}\,dx} S^{-1/2} = 3\left(\frac{L_*}{4\pi}\right)^{1/2}\left(\frac{H_0}{c}\right)\frac{\int_0^\infty \phi(x)x^2\,dx}{\int_0^\infty \phi(x)x^{3/2}\,dx} S^{-1/2}. \tag{A9}$$

Let us carefully examine equation (A9). First, the dependence of the mean redshift on the limiting flux density S is a power of $-1/2$. Also, it has the same order of dependence on L_*. In contrast, the integral part of equation (A9) has an important meaning. Since this part depends on the second-order moment, the tail of the LF affects the value very strongly. As we mentioned, we integrate over the (normalized) luminosity up to a certain very large value, and this part is a ratio between the moments of order $3/2$ and 2. Hence the contribution from a large value of x controls the value. Consequently, the mean redshift $\langle z \rangle_{>S}$ is very sensitive to the LF shape.

This aspect is clearly seen in the comparison of the expected redshift distributions in NUV and 60 μm calculated from the LFs and the limiting flux density or magnitude, because the shapes of the LFs at these wavelengths are very different (Buat & Burgarella 1998; Takeuchi et al. 2005). We show the comparison in Figures 2b and 2c. In these figures we fix the limiting flux density at 60 μm to be 0.6 Jy, while we change the limiting magnitude from $AB_{NUV} = 16.0$ mag (the actual value we adopt in this work) to 18.0 mag. The medians for the two wavelengths are very different when we adopt a limiting value of $AB_{NUV} = 16.0$ mag. Only when we adopt a limiting value of $AB_{NUV} = 18.0$ mag, which corresponds to a very sensitive survey, do the median values for the NUV- and FIR-selected samples become more similar.

APPENDIX B

ESTIMATING THE BIRTHRATE PARAMETER

Boselli et al. (2001) give a detailed recipe for estimating $\langle \mathrm{SFR} \rangle$, based only on observable quantities and/or adopted values for the parameters (see Gavazzi et al. 1996). Here we follow their prescriptions, using the H-band luminosity to estimate the past-averaged SFR and the same parameters that they used:

$$b = \frac{\mathrm{SFR} \times t_0 \times (1 - R)}{L_H \times (M_{\mathrm{tot}}/L_H) \times \mathrm{DM}_{\mathrm{cont}}}, \tag{B1}$$

where SFR in this work is averaged over 10^8 yr, t_0 is the age of the disk (assumed to be equal to 13 Gyr), R is the fraction of gas reinjected by stars through stellar winds into the interstellar medium during their lifetime (taken to be equal to 0.3 for a Salpeter IMF), L_H is the H-band luminosity estimated as $\log L_H = 11.36 - 0.5H + 2\log D$ (in solar units) where D is the distance to the source (in Mpc), M_{tot} is the dynamical mass at the B-band 25 mag arcsec^{-2} isophotal radius, M_{tot}/L_H is taken to be constant and equal to 4.6 (in solar units), and $\mathrm{DM}_{\mathrm{cont}}$ is the dark matter contribution to the M_{tot}/L_H ratio at the optical radius, assumed to be equal to 0.5.

---

[15] Note that this is different from the quantity defined by eq. (5.134) of Peebles (1993).

REFERENCES

Balland, C., Devriendt, J. E. G., & Silk, J. 2003, MNRAS, 343, 107
Bell, E. F. 2003, ApJ, 586, 794
Bertin, E., & Arnouts, S. 1996, A&AS, 117, 393
Boselli, A., Gavazzi, G., Donas, J., & Scodeggio, M. 2001, AJ, 121, 753
Brinchmann, J., & Ellis, R. S. 2000, ApJ, 536, L77
Buat, V., & Burgarella, D. 1998, A&A, 334, 772
Buat, V., Donas, J., Milliard, B., & Xu, C. 1999, A&A, 352, 371
Buat, V., & Xu, C. 1996, A&A, 306, 61
Buat, V., et al. 2005, ApJ, 619, L51
Burgarella, D., Buat, V., & Iglesias-Páramo, J. 2005, MNRAS, 360, 1413
Cardelli, J. A., Clayton, G. C., & Mathis, J. S. 1989, ApJ, 345, 245
Cardiel, N., Elbaz, D., Schiavon, R. P., Willmer, C. N. A., Koo, D. C., Phillips,
    A. C., & Gallego, J. 2003, ApJ, 584, 76
Charmandaris, V., Le Floc'h, E., & Mirabel, I. F. 2004, ApJ, 600, L15
Chary, R., & Elbaz, D. 2001, ApJ, 556, 562
Cowie, L. L., Songaila, A., Hu, E. M., & Cohen, J. G. 1996, AJ, 112, 839
Dale, D. A., Helou, G., Contursi, A., Silbermann, N. A., & Kolhatkar, S. 2001,
    ApJ, 549, 215
Devriendt, J. E. G., & Guiderdoni, B. 2000, A&A, 363, 851
Flores, H., et al. 1999, ApJ, 517, 148
Garnett, D. R., & Shields, G. A. 1987, ApJ, 317, 82
Gavazzi, G., Pierini, D., & Boselli, A. 1996, A&A, 312, 397
Gordon, K. D., Calzetti, D., & Witt, A. N. 1997, ApJ, 487, 625
Gordon, K. D., Clayton, G. C., Witt, A. N., & Misselt, K. A. 2000, ApJ,
    533, 236
Guiderdoni, B., & Rocca-Volmerange, B. 1987, A&A, 186, 1
Heavens, A., Panter, B., Jimenez, R., & Dunlop, J. 2004, Nature, 428, 625
Heckman, T. M., et al. 2005, ApJ, 619, L35
Hirashita, H., Buat, V., & Inoue, A. K. 2003, A&A, 410, 83
Iglesias-Páramo, J., Buat, V., Donas, J., Boselli, A., & Milliard, B. 2004, A&A,
    419, 109
Jarrett, T. H., Chester, T., Cutri, R., Schneider, S., Skrutskie, M., & Huchra, J. P.
    2000, AJ, 119, 2498
Kennicutt, R. C. 1998, ARA&A, 36, 189
Kong, X., Charlot, S., Brinchmann, J., & Fall, S. M. 2004, MNRAS, 349, 769

Leitherer, C., et al. 1999, ApJS, 123, 3
Lilly, S. J., Le Fèvre, O., Hammer, F., & Crampton, D. 1996, ApJ, 460, L1
Lonsdale Persson, C. J., & Helou, G. 1987, ApJ, 314, 513
Lynden-Bell, D. 1971, MNRAS, 155, 95
Madau, P., Ferguson, H. C., Dickinson, M. E., Giavalisco, M., Steidel, C. C., &
    Fruchter, A. 1996, MNRAS, 283, 1388
Martin, D. C., et al. 2005a, ApJ, 619, L1
———. 2005b, ApJ, 619, L59
Meurer, G. R., Heckman, T. M., & Calzetti, D. 1999, ApJ, 521, 64
Morrissey, P., et al. 2005, ApJ, 619, L7
Moshir, M., et al. 1990, IRAS Faint Source Catalog (ver. 2.0; Greenbelt: NASA)
Panuzzo, P., Bressan, A., Granato, G. L., Silva, L., & Danese, L. 2003, A&A,
    409, 99
Peebles, P. J. E. 1993, Principles of Physical Cosmology (Princeton: Princeton
    Univ. Press)
Rowan-Robinson, M., et al. 1997, MNRAS, 289, 490
Salim, S., et al. 2005, ApJ, 619, L39
Saunders, W., et al. 2000, MNRAS, 317, 55
Sauvage, M., & Thuan, T. X. 1992, ApJ, 396, L69
Scalo, J. M. 1986, Fundam. Cosmic Phys., 11, 1
Schiminovich, D., et al. 2005, ApJ, 619, L47
Schlegel, D. J., Finkbeiner, D. P., & Davis, M. 1998, ApJ, 500, 525
Steidel, C. C., Adelberger, K. L., Giavalisco, M., Dickinson, M., & Pettini, M.
    1999, ApJ, 519, 1
Sullivan, M., Mobasher, B., Chan, B., Cram, L., Ellis, R., Treyer, M., &
    Hopkins, A. 2001, ApJ, 558, 72
Takeuchi, T. T., Buat, V., & Burgarella, D. 2005, A&A, 440, L17
Takeuchi, T. T., Yoshikawa, K., & Ishii, T. T. 2000, ApJS, 129, 1
———. 2003, ApJ, 587, L89
Vijh, U. P., Witt, A. N., & Gordon, K. D. 2003, ApJ, 587, 533
Wang, B., & Heckman, T. M. 1996, ApJ, 457, 645
Witt, A. N., & Gordon, K. D. 2000, ApJ, 528, 799
Wyder, T. K., et al. 2005, ApJ, 619, L15
Zaritsky, D. 1993, PASP, 105, 1006